Available online at www.CivileJournal.org

Civil Engineering Journal

(E-ISSN: 2476-3055; ISSN: 2676-6957)

Vol. 9, No. 02, February, 2023

Bond–slip Behaviour of NSM GFRP Bars in Reinforced Recycled-Aggregate Concrete: Experiments and a Modified Model

Anh-Tuan Le [1, 2], Thuy Ninh Nguyen [1, 2], Vui Van Cao [1, 2*]

[1] *Faculty of Civil Engineering, Ho Chi Minh City University of Technology (HCMUT), District 10, Ho Chi Minh City, Vietnam.*

[2] *Vietnam National University Ho Chi Minh City, Linh Trung Ward, Thu Duc City, Ho Chi Minh City, Vietnam.*

Received 15 November 2022; Revised 06 January 2022; Accepted 19 January 2023; Published 01 February 2023

Abstract

Bond-slip behaviour of glass fiber-reinforced polymer (GFRP) bars embedded in conventional concrete has been widely investigated. In contrast, the bond-slip behaviour of near-surface mounted (NSM) GFRP bars bonded in reinforced recycled aggregate concrete (RAC) seems to be less explored, while recycled materials have been increasingly used due to reasons of environmental pollution and resource exhaustion. This study aimed to experimentally and theoretically examine the bond-slip behaviour of NSM GFRP bars in reinforced RAC under monotonic and cyclic loadings. To achieve this aim, twenty-four tests were performed, which were divided into two groups by monotonic and cyclic loadings. In each group, twelve tests were performed on ten reinforced RAC specimens and two reinforced normal aggregate concrete (NAC) specimens. The test results confirmed the brittle shear failure of concrete in the proximity of a resin-concrete surface. Bond-slip behaviour can be characterized by nonlinear and linear branches, in which the linear branch dominates the behaviour. Under monotonic and cyclic loadings, the average slips of GFRP bars in reinforced RAC were 0.238 and 0.284 mm, and their coefficients of variation (COV) were relatively large at 0.142 and 0.130, respectively. In contrast, ultimate loads had a relatively low COV of around 0.038. The effect of cyclic loading significantly increased the ultimate slip by 19.3%, whereas it negligibly reduced the ultimate load; consequently, the stiffness was reduced by 19.4%. A modified smooth model was proposed to predict the bond-slip behaviour of NSM GFRP bars in reinforced RAC under monotonic and cyclic loadings. The simplicity and accuracy of the model can be useful for engineers in structural retrofitting using NSM FRP technique.

Keywords: GFRP; Near-Surface Mounted; Bond-slip Behaviour; Recycled-Aggregate Concrete; Strengthening.

1. Introduction

Near-surface mounted fiber-reinforced polymer (NSM FRP) is a promising retrofitting technique that has attracted researchers worldwide. NSM FRP has been investigated for beams [1, 2], columns [3], and structures [4]. This method has been proven to be more effective than the externally bonded method [5–7] because NSM FRP works with inner concrete; thus, FRP is more efficiently exploited, avoiding premature debonding failure. Additionally, the NSM technique has better fire resistance and less damage because FRP is protected by concrete. The most important aspect of the NSM technique is the bond between FRP and concrete. Bond-slip behaviour of NSM FRP plays an important role in the behaviour of concrete components or structures retrofitted with NSM FRP [8, 9].

In the last decades, numerous studies have been performed on several different aspects/issues of NSM FRP [10]. FRP strips and FRP bars can be commonly used for NSM retrofitting. Regarding NSM using FRP strips, Hassan &

* Corresponding author: cvvui@hcmut.edu.vn

http://dx.doi.org/10.28991/CEJ-2023-09-02-01

Rizkalla [11] experimentally and analytically investigated the bond-slip behaviour of NSM CFRP strips in concrete beams, and an analytical model was proposed to estimate the shear stress at the interface. José & Joaquim [12] investigated the bond between NSM CFRP laminate strips and concrete. The results indicated that the pull-out force increased with the increase in bond length, whereas the concrete strength only marginally affected the bond-slip behaviour. Rashid et al. [13] investigated the intermediate crack debonding interaction of NSM FRP and external bonded (EB) FRP with concrete cover. The results indicated that EB plates and adjacent plates exhibited no interaction. However, NSM plates and adjacent plates exhibited strong interaction when the lateral spacing was less than 53 mm. Oehlers et al. [14] used NSM FRP strips to improve the intermediate crack debonding capacity and found that embedding NSM FRP strips substantially increased the debonding resistance and slip capacity. Vasquez & Seracino [15] assessed the performance of available analytical models for predicting the debonding of NSM FRP strips. Zhang et al. [16] conducted 3D finite modeling and indicated that the concrete strength and the height-to-width ratio of grooves played important roles in bond-slip behaviour. A bond-slip model, which was the product of a power function and a trigonometric function, was proposed. Zhang et al. [17] developed models of bond strength and bond length for NSM CFRP strips in concrete. These models were validated by comparing them with the experimental results collected in the literature. Dai et al. [18] used a new analytical method to develop a bond-slip model of an NSM FRP sheet. The interesting point was that this method avoided using many strain gauges installed on FRP to obtain the strain distribution. This method used the relationship between load and loaded-end slip to derive a bond-slip model at the interface.

Regarding NSM retrofitting using FRP bars, Lorenzis et al. [19] studied the bond behaviour between NSM FRP rods and concrete in structures and found that the bond strength was affected by the surface conditions of the FRP bars. Lorenzis et al. [20] used a modified pull-out test to investigate the bond behaviour between NSM FRP rods and concrete, in which the issue of eccentricity was eliminated. The results indicated that the failure mode was at the epoxy-concrete interface. In addition, the ultimate load of specimens using cement mortar was lower than that using epoxy. Galati and Lorenzis [21] experimentally investigated the effect of different parameters on the bond behaviour of NSM FRP bars in concrete. The results showed that local bond strength moderately increased as the groove dimensions increased. There was no reduction in bond strength when the clear distance of the square groove size was equal to or larger than twice the groove dimension. Shehab et al. [22] studied the bond-slip behaviour of NSM FRP bars with consideration of different parameters and freeze/thaw cycles. The results indicated that the increase in groove size insignificantly increased the ultimate load, whereas the tensile strength of concrete was an important factor that governed the failure mode. The variation in temperature due to freeze/thaw cycles caused hair cracks in adhesive materials, which were then governed by the failure mode. Sharaky et al. [23] studied the effects of material and construction details on the bond behaviour between NSM FRP bars and concrete. Different failure modes were observed. For square grooves, failure of the bar-epoxy interface was delayed, and the ultimate load increased by 14.8% when the groove size increased from 1.5 to 2 times the diameter of the FRP bar. Sharaky et al. [24] experimentally investigated different parameters that affected the bond behaviour of NSM FRP bars in concrete and found that adhesive properties, FRP bar diameter, and bar surface treatment critically affected the bond capacity and failure mode.

Kalupahana et al. [25] investigated the bond characteristics of NSM CFRP bars and found that bars with a lower ratio of cross-sectional area to perimeter, e.g., rectangular bars, exhibited higher effectiveness. This ratio significantly affected the failure mode in the form of separation of concrete cover. Lee et al. [26] studied the bond performance of different NSM FRPs in concrete and found that GFRP bars had higher strength but lower slip than CFRP bars. The pull-out load and material efficiency of the strip were higher than bars with other sections. Caro et al. [27] experimentally investigated the bond behaviour of deep embedment CFRP and GFRP in concrete. The results indicated that the pull-out capacity increased while the bond strength and initial stiffness decreased with the increase in embedded length. A mathematical model was proposed to predict the bond strength of deep embedment FRP, and good accuracy with the experimental results was achieved. Gómez et al. [28] numerically studied the bond-slip behaviour of NSM FRP in concrete, considering the shape of the local bond-slip rule and its parameters. The results indicated that the shape of the bond–slip rule exhibited a marginal effect on the slip of FRP. In contrast, the friction branch significantly affected the distribution of bond stress and slip at the ultimate state.

In 2021, Gómez et al. [29] experimentally and numerically predicted the performance of NSM CFRP laminates in RC members subjected to sustained loading for 1000 h. A time-dependent bond-slip model based on strength reduction and creep coefficient was proposed. The creep coefficient governed the time-dependent bond-slip behaviour of specimens subjected to 15% of the ultimate load. Zhang & Xue [30] used artificial intelligence techniques and available empirical models to predict the bond strength of NSM FRP. The results showed that models based on artificial intelligence techniques had a higher determination coefficient but lower other statistical indices compared with those based on available empirical models. The increase of bond length, FRP stiffness, ratio of depth to width of grooves, and concrete strength increased the bond strength. Slaitas & Valivonis [31] examined bond strength models of NSM FRP in RC members at the ultimate stage. An analytical method without using failure criteria or experimental fracture energy was proposed. The reduction of member stiffness due to slip between FRP and concrete was evaluated for use in predicting the load-carrying capacity of FRP-retrofitted members.

Wang & Cheng [32] performed 24 pull-out tests of NSM CFRP rods and strips in concrete to investigate the strength and characteristics of the bond. The results indicated that bond behaviour was positively affected by the strengths of adhesive and concrete. An analytical trilinear model was proposed and verified through good agreement with the experimental results. Aghamohammadi et al. [33] performed a reliability study on three models of bond strengths of NSM FRP bars and strips in concrete. Available data from 451 tests was collected and analyzed. The findings indicated that significant improvements were needed to the considered bond models of strength reliability related to the existing factors of strength reduction. Li et al. [34] experimentally investigated the effect of strain rate on bond behaviour between BFRP bars and RAC. The results showed that the increase in strain rate decreased the bonding mechanism of interlocking and friction. The increase in strain rate improved bond behaviour and weaken the bond mechanism. Formulae were proposed to estimate the bond behaviour under various strain rates. Yazdani et al. [35] considered data correlation to estimate FRP-to-concrete bond capacity models. Extensive data collected from the literature was used to improve the reliability and accuracy of such models. The method of mixed-effects regression was to analyze clustered databases, and the data correlation significantly improved its reliability and decreased the uncertainty of models.

Recently, Mosallam et al. [36] performed 15 pull-out tests of NSM CFRP strips on U-shaped RC specimens. The results indicated that the geometry of the grooves significantly influenced the bond strength and failure mode. FRP with lower moduli and higher rupture strains could improve the stiffness and performance of the NSM system. Aljidda et al. [37] experimentally and analytically studied the bond performance of NSM FRP bars, accounting for different parameters such as FRP types, bar surfaces, adhesive types, and bond length. The results confirmed the outperformance of NSM-Gel adhesive on bond strength compared with other adhesives. The bond strength of NSM CFRP was the highest, while the bond strengths of NSM BFRP and GFRP were similar. An analytical bond-slip model of NSM FRP bars was calibrated. Reviews on FRP strengthening RC members using groove methods have been conducted by researchers such as Sanginabadi et al. [38].

The fast growth of infrastructure has resulted in a high demand for building materials. To meet this demand, natural resources are being heavily exploited, causing concerns about environmental pollution and resource exhaustion. Therefore, recycled materials are becoming increasingly necessary for sustainable development. Construction waste, e.g., old concrete from demolished or damaged buildings, can be recycled. Different aspects of recycled-aggregate concrete (RAC) have been investigated, e.g., mechanical properties [39–48], strengths of structural components [46, 49, 50], and frame structures [51].

There have been several studies on the properties of RAC, NSM FRP in normal-aggregate concrete (NAC), and NSM FRP in reinforced NAC, as reviewed above. In contrast, studies on the bond-slip behaviour of NSM FRP bars in reinforced RAC are hardly found in the literature. Furthermore, in practice, loads often vary with time, e.g., a live load acting on a floor and then transferring to beams, traffic loads acting on a bridge girder, etc. Therefore, not only monotonic loading but also cyclic loading should be used to investigate the bond-slip behaviour of NSM FRP bars in reinforced RAC. A sound understanding of the bond-slip behaviour of NSM FRP bars in reinforced RAC should be developed to provide technical information for engineers who work in the field of FRP retrofitting. This study aimed to experimentally and theoretically examine the bond-slip behaviour of NSM GFRP bars in reinforced RAC under monotonic and cyclic loadings. To achieve this aim, 24 pull-out tests of NSM GFRP bars under monotonic and cyclic loadings were performed. These 24 tests included 20 tests on reinforced RAC and 4 tests on reinforced NAC. The test results were analyzed to evaluate the different mechanical properties and bond-slip behaviour of NSM FRP bars in reinforced RAC, highlighting the effect of cyclic loading. Additionally, a modified smooth bond-slip model for NSM FRP bars in reinforced RAC was proposed. The results obtained from this model showed good agreement with the experimental results. The simplicity and accuracy of the model make it useful for structural engineers in retrofitting structures using NSM FRP technique.

2. Experimental Program

2.1. Materials and Specimens

The composition of RAC and NAC was similar and is shown in Table 1. RAC was made of forty-year-old concrete that was crushed to use as coarse aggregate, whereas the coarse aggregate of NAC was made of normal stone. Figure 1 shows the grading curves of fine and coarse aggregates, in which the upper and lower bounces adopted in TCVN 7570 [52] were also plotted. During the concrete casting, three standard cylinder samples (diameter = 150 mm, height = 300 mm) of each concrete type were taken. The average compressive strengths of three NAC and RAC concrete samples at the age of 28 days were 26.3 MPa and 22.4 MPa, respectively. Steel ϕ6 and ϕ14 were used for transverse and longitudinal reinforcement, respectively. The thickness of concrete cover was 30 mm measured to the center of stirrups. GFRP bar ϕ10 was used for the tests. Three specimens of ϕ10 GFRP bars were taken to test the tensile strengths. Resin TCK 510 R was used for NSM retrofitting. The mechanical properties of the resin provided by the manufacturer are the elastic modulus of 2.76 GPa, the tensile strength of 40.08 MPa, and the compressive strength of 128 MPa.

Table 1. Concrete mix

Material	Mass/volume per m^3
PC40 cement	300 kg
Coarse aggregate, D_{max} = 20 mm	1151 kg
Sand ≤ 2.5 mm	863 kg
Water	131 liter

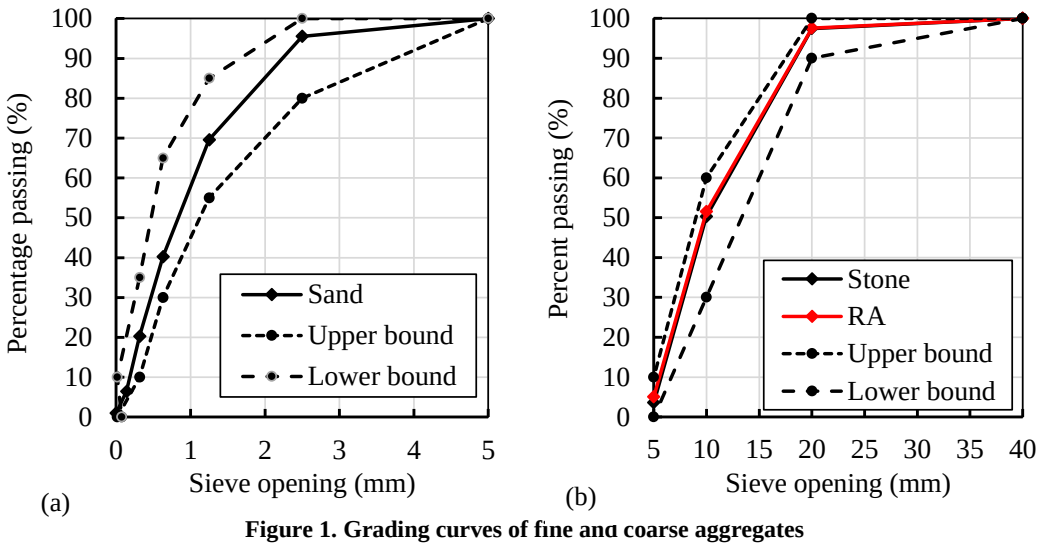

Figure 1. Grading curves of fine and coarse aggregates

There were twelve reinforced concrete (RC) blocks, in which ten blocks were of reinforced RAC and two blocks were of reinforced NAC. These twelve blocks were labeled as 'Concrete type'-'Number'. Concrete types were RAC and NAC and the number varied from 01 to 10 for RAC blocks and 01 to 02 for NAC blocks. Each concrete block designed with two pull-out tests [53] was adopted in this study. The top sides of specimens were used for monotonic loading, whereas the bottom sides of specimens were used for cyclic loading. The structure of specimen labels was 'Concrete type'-'Number'-'Loading type'. 'Loading type' was M and C, representing monotonic and cyclic loadings, respectively. Table 2 shows 24 specimens which were made from ten RAC and two NAC blocks.

Table 2. Names and loading types of specimens

No.	Group	Specimen	Loading	Group
1	RAC	RAC-01-M	Monotonic	M
2		RAC-02-M		
3		RAC-03-M		
4		RAC-04-M		
5		RAC-05-M		
6		RAC-06-M		
7		RAC-07-M		
8		RAC-08-M		
9		RAC-09-M		
10		RAC-10-M		
11	NAC	NAC-01-M		
12		NAC-02-M		
13	RAC	RAC-01-C	Cyclic	C
14		RAC-02-C		
15		RAC-03-C		
16		RAC-04-C		
17		RAC-05-C		
18		RAC-06-C		
19		RAC-07-C		
20		RAC-08-C		
21		RAC-09-C		
22		RAC-10-C		
23	NAC	NAC-01-C		
24		NAC-02-C		

Figure 2 shows the specimens at different preparation stages. Figures 2-a and 2-b show reinforced RAC and NAC blocks before and after grooving, respectively. Figure 2-c shows the specimens which were used for monotonic loading. After the tests of specimens under monotonic loading (Figure 2-c) were completed, NSM GFRP bars were installed on the other sides of these reinforced concrete blocks as shown in Figure 2-d to use for cyclic loading. Figure 3 shows dimensions 150×200×500 mm of the concrete blocks and the installation of NSM GFRP bars. Figure 3-b shows locations of FRP bars for monotonic and cyclic loading tests. The bond length was selected to be $L_{bonded} = 12 \times d_{frp} = 120$ mm, where d_{frp} is the diameter of GFRP bar, which was used by previous researchers [22]. The unbonded length $L_{unbonded} =$ 50 mm, which was used by Ceroni et al. [53, 54], was adopted. Singh et al. [55] and ACI 440.2R-17 [56] recommended a minimum size of $1.5 \times d_{frp}$; thus, the groove size of 15 × 15 mm was used in this study. Figure 3c shows the flowchart of the above-described experiments.

(a) Reinforced NAC (left) and RAC blocks

(b) Reinforced blocks after grooving

(c) Specimens for monotonic loading

(d) Specimens for cyclic loading

Figure 2. Specimens

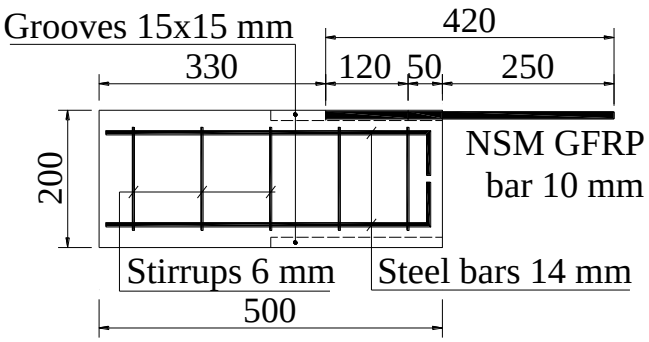

(a) Specimens and dimensions

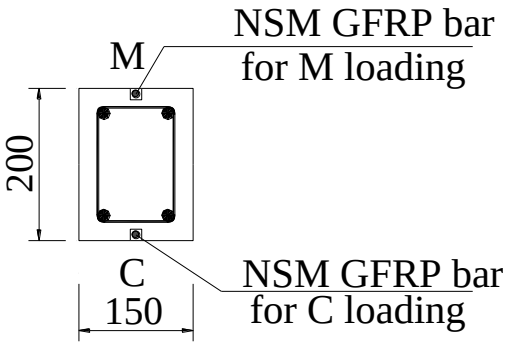

(b) Cross section

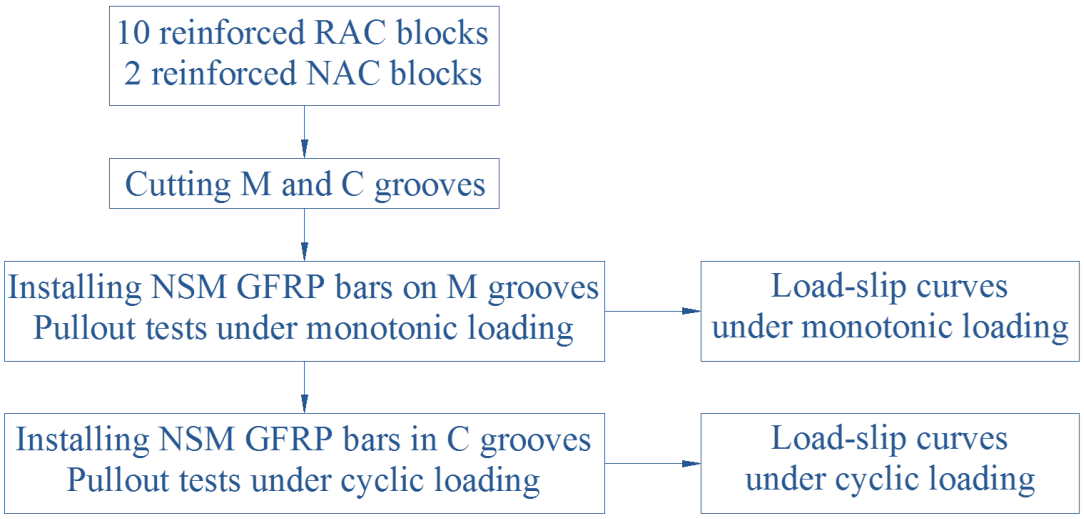

(c) Flowchart of the experiments

Figure 3. NSM GFRP specimens (dimensions are in mm)

2.2. Test Setup

Figures 4-a and 4-b show general and close views of the experiment setup, respectively, which is outlined in Figure 4-c. The testing system included a strong steel frame, two support reactions, a hydraulic jack, a clamp, a load cell, a load transfer system, and two rollers. The load cell was attached to the movable end of the hydraulic jack to measure the load exerting on the load transferring system. The load-transferring system included four ϕ16 high-strength steel bars and two steel plates. This load transferring system converted the compression force of the hydraulic jack to the tension force acting on the GFRP bar. There were two rollers to support the weight of the load-transferring system. With this system, the lateral load of the hydraulic jack was transferred to the GFRP bar, while the weight of the load transfer system was supported by the two rollers. The clamp was specially designed using a hollow steel tube with a thickness of 10 mm and an outer diameter of 38 mm. One end of this steel tube was fixed to the load transfer system, while the other end was inserted by the GFRP bar into the hollow. There are several bolts on the side of this hollow steel tube. Inside the steel tube, there was a half of other small steel tube with a thickness of 3.5 mm. When a specimen was installed on the testing system, the GFRP was in the 38 mm steel tube, and the small half-steel tube was in between the GFRP bar and the bolts. When the bolts were tightened, the forces of these bolts exerted on the small half-steel tube. The function of this small half-steel tube was to distribute the forces of the bolts in the form of pressure on the GFRP bar (not the concentrated forces directly from the bolts). With this mechanism, the GFRP bar can be fixed to the hollow steel tube while its failure is avoided.

(a) General view

(b) Close view

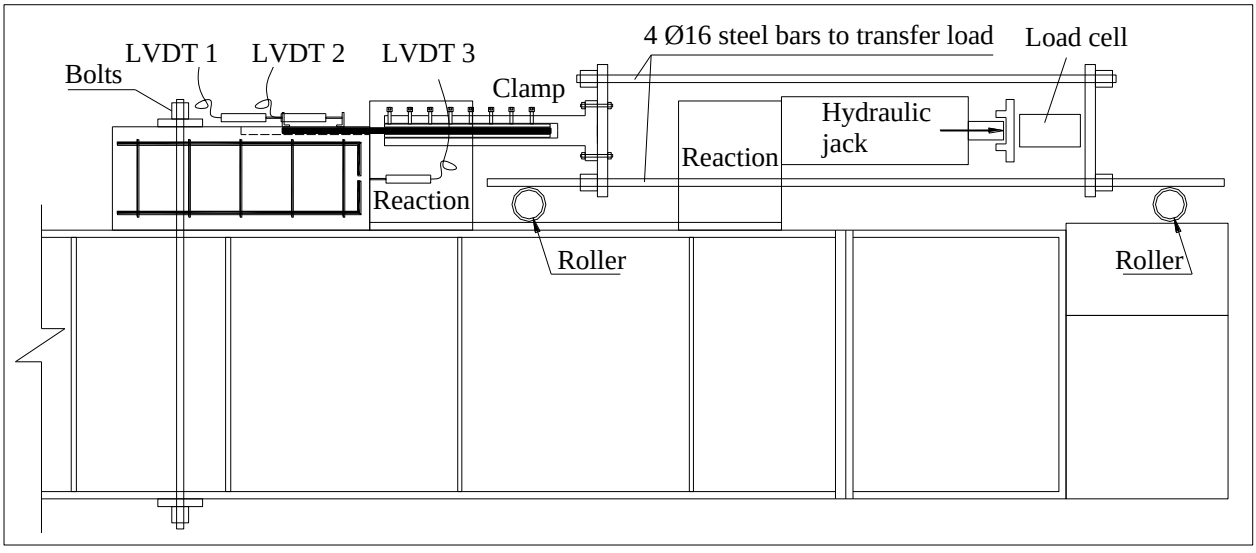

(c) Outline

Figure 4. Experiment setup

The measurement system included three LVDTs and a load cell. LVDT 1 and LVDT 2 were installed to measure the displacements of free end ($u_{freeend}$) and loaded end ($u_{loadedend}$), respectively. LVDT 3 was installed to measure the displacement of the concrete block (u_{block}). The accuracy of LVDTs was 10^{-3} mm, which was adequate to measure the relatively small displacements. The slips of free end ($s_{freeend}$) and loaded end ($s_{loadedend}$) were calculated based on Equations 1 and 2:

$$s_{loadedend} = u_{loadedend} - u_{block} \quad (1)$$

$$s_{freeend} = u_{freeend} - u_{block} \quad (2)$$

2.3. Loading and Testing Procedure

The monotonic loading can be useful for the case of static loading while the cyclic loading can be useful for the case of repeated/varied loading in practice. The average increasing load was approximately 50 N/s. If many cycles were applied, it could cause overlap and difficulty in analysing the degradation of mechanical properties. The cyclic loading used in this study was as follows. The increment interval of load was selected to be ΔP = 2500 N; therefore, the peak load of the i^{th} cycle was $i \times \Delta P = i \times 2500$ N. In each cycle, the load was increased from 0 up to the peak load of that cycle, and then the load was slowly released to zero [57]. Figure 5 shows the cyclic loading history described above. This loading procedure was applied until the specimen failed. It should be noted that, after the specimen was installed, the specimen was loaded to 1 kN and then released to zero. The goal of this step was to eliminate any contact-related errors. After this step, the main testing procedure was conducted.

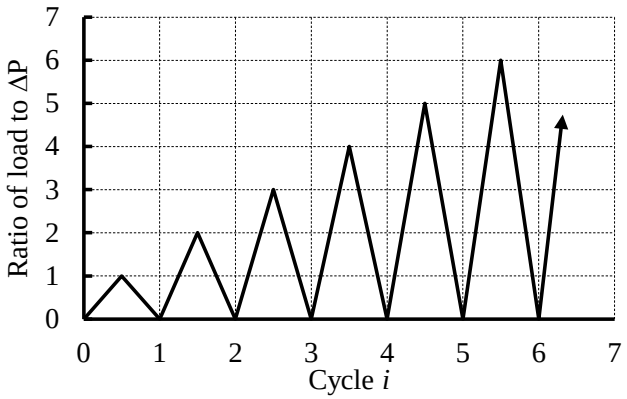

Figure 5. Cyclic loading history

3. Experimental Results

3.1. Failure Modes

Figure 6-a shows a typical failure mode of specimens on the testing system. Figures 6-b and 6-c show the failure of specimens under monotonic and cyclic loadings after testing, respectively. All specimens had brittle failure. When failure occurred, NSM GFRP bars were unable to resist any load, and the load sharply dropped to zero. During the loading process, the load continuously increased to the ultimate, and there is no descending branch. When the specimens failed, a small explosive sound was heard, and pieces of concrete shot toward the loading side and left/right sides. Failure in the form of GFRP rupture was not observed in the tests.

(a) Typical failure of specimens on the testing system

(b) Failure of specimens under monotonic loading

(c) Failure of specimens under cyclic loading

Figure 6. Failure modes

It should be noted that the failure modes shown in Figures 6-b and 6-c were the states of specimens after taking from the testing system. The concrete in the proximity to the GFRP bars disintegrated into several pieces, forming an inclined failure surface. However, the failure mode of the specimen on the testing apparatus (Figure 6-a) shows a clear failure surface around the resin. This can be evidence that specimens failed in the form of shear failure, with the failure surface in concrete around the resin. When specimens failed, the GFRP bar, together with the resin, rapidly moved toward the loading side. During this rapid movement, the rough surface of the resin exerted a lateral stress on the concrete, disintegrating it into small pieces. This process occurred very quickly; thus, the failure should be considered at the beginning state of this process rather than at the state after taking specimens from the testing apparatus. Therefore, the concept of shear failure in the resin was adopted to compute the shear stress in this study.

3.2. Load–Slip Curves under Monotonic Loading

Figures 7-a to 7-k show load-slip curves of RAC specimens under monotonic loading. The axis limits were set to be the same for visual comparison. Generally, the ultimate slips of specimens are quite different. This difference was expected and was a reason for designing ten specimens in each group to increase the accuracy. The load-slip curves can be generally divided into two branches: branch 1 when the load varies from 0 to about 5 kN, and branch 2 when the load varies from about 5 kN to the ultimate. The slope of branch 1 is much larger than that of branch 2. Figures 7-l and 7-m show the load-slip curves of the free end and loaded end of specimens NAC-01-M and NAC-02-M, respectively. When Figures 7-l to 7-m are compared with Figures 7-a to 7-k, the ultimate loads of NAC specimens are much higher than those of RAC specimens. Quantitative comparisons are presented in Section 4.

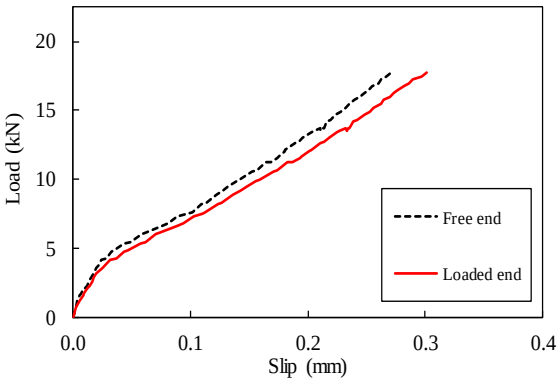

(a) RAC-01-M

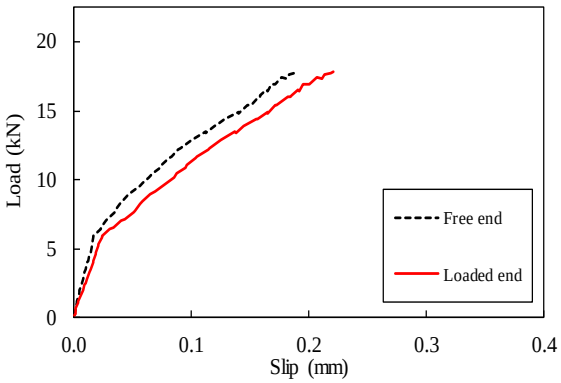

(b) RAC-02-M

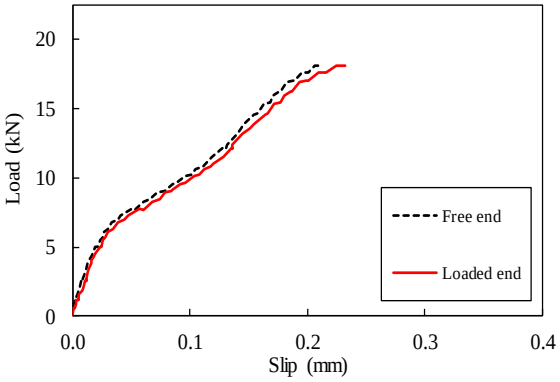

(c) RAC-03-M

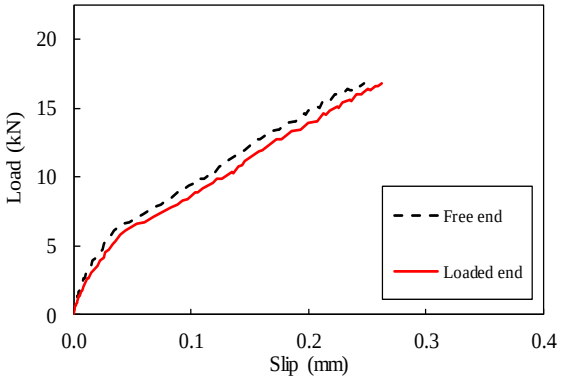

(d) RAC-04-M

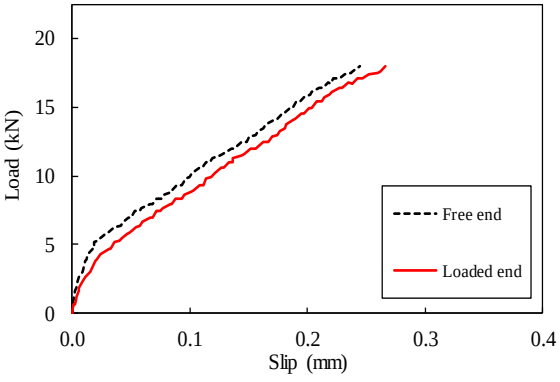

(e) RAC-05-M

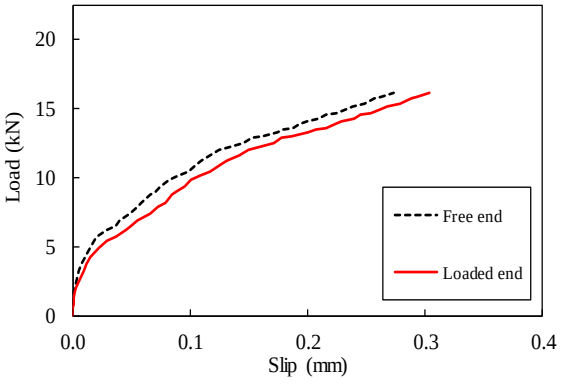

(f) RAC-06-M

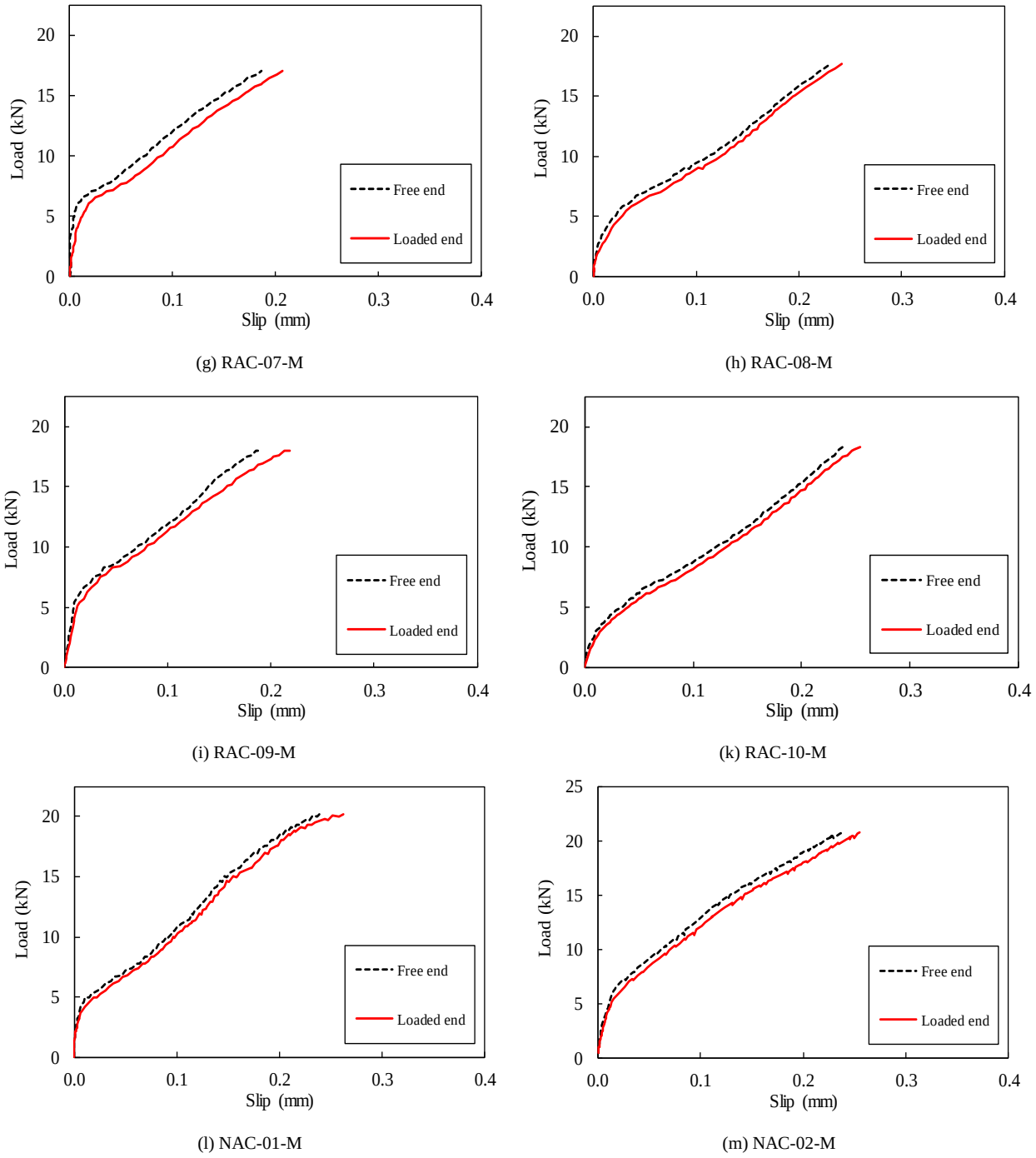

Figure 7. Load−slip curves of specimens under monotonic loading

3.3. Load–Slip Curves under Cyclic Loading

Figures 8a to 8-k show the load−slip curves of RAC specimens under cyclic loading. The axis limits were set to be the same for visual comparison. Overall, the ultimate loads, ultimate slips, and number of cycles are different from specimens to specimens. However, the similar characteristic is as follows. The stiffness when the load is under 5 kN is much larger than that when the load is above 5 kN. The envelop curves were determined and used for analyses of different mechanical properties. These ten envelope curves were also used to compute the average curve, which is used for comparisons in the later sections. Figures 8-l and 8-m show the load−slip curves of NAC specimens NAC-01-C and NAC-02-C, respectively. It is clear that the ultimate loads, ultimate slips, and the number of cycles are much higher than those of RAC specimens. Detailed comparisons are presented in Section 4.

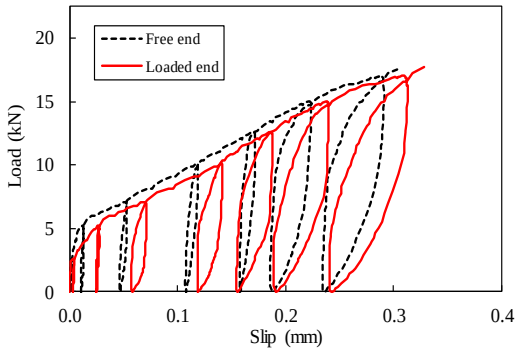

(a) RAC-01-C

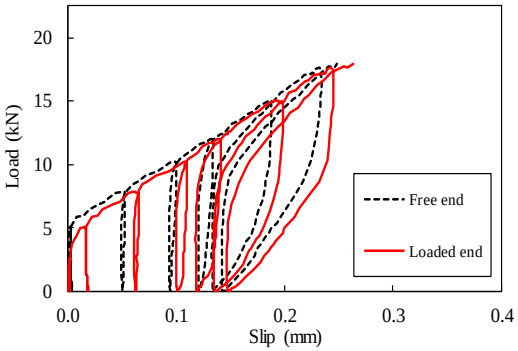

(b) RAC-02-C

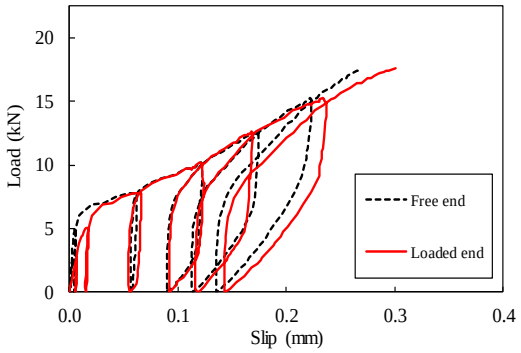

(c) RAC-03-C

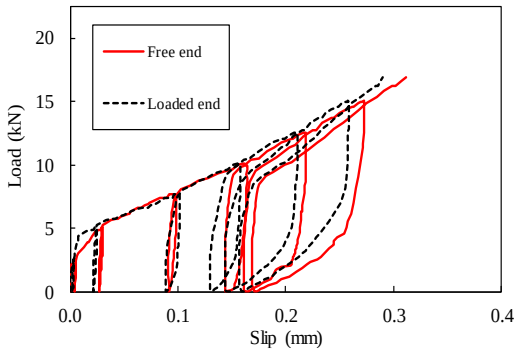

(d)

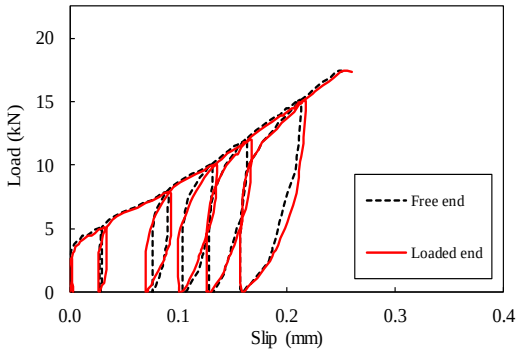

(e) RAC-05-C

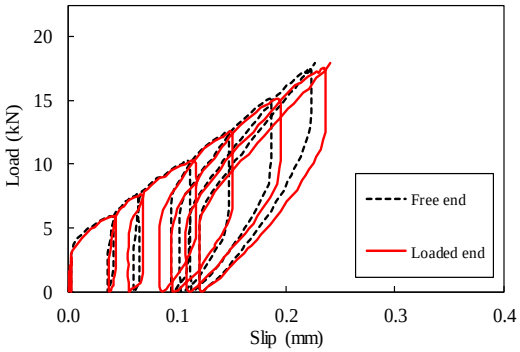

(f) RAC-06-C

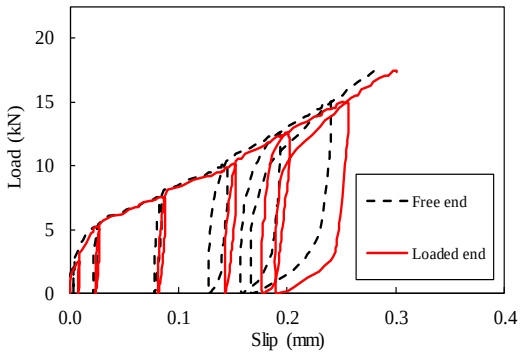

(g) RAC-07-C

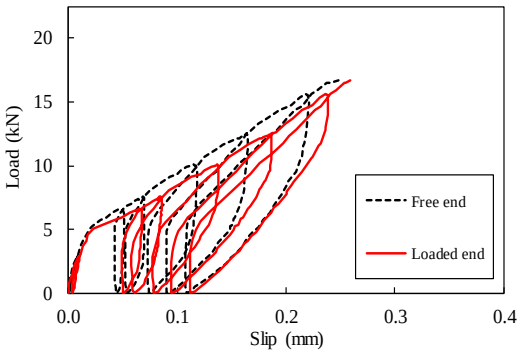

(h) RAC-08-C

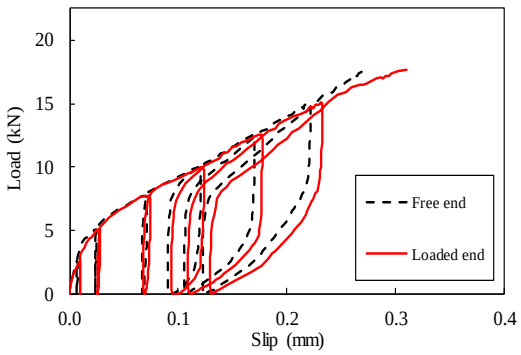

(i) RAC-09-C

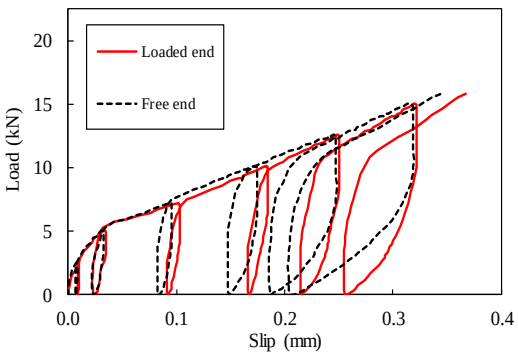

(k) RAC-10-C

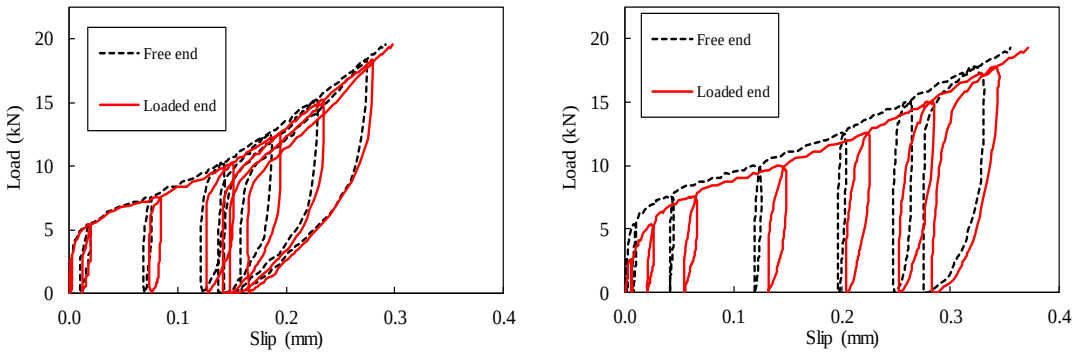

(l) NAC-01-C (m) NAC-02-C

Figure 8. Load–slip curves of specimens under monotonic loading

4. Analyses of the Experimental Results

4.1. Analyses of Load–Slip Curves under Monotonic Loading

For ten RAC specimens, ten load–slip curves of loaded ends were used to compute the average curve. The procedure to obtain the average curve is described as follows. First, the minimum load of ten maximum loads was determined. Then, the domain of load (from zero to the just-mentioned minimum load) was divided into several intervals with an increment of 0.05 kN. At a certain load, for example, 2 kN, there were ten corresponding loaded-end slips, which were obtained from ten load-loaded-end slip curves. Then, the average and standard deviation of these ten slips were computed. This step was repeated for all load intervals; consequently, the average and 'average ± one standard deviation' load-slip curves were obtained. This procedure was also applied for ten load-free-end slip curves to obtain the corresponding average and 'average ± one standard deviation' curves. Figure 9-a shows ten curves of the loaded end and the corresponding average curve. The two curves corresponding to 'average ± one standard deviation' are also plotted in this figure. Similarly, Figure 9-b shows ten curves of free ends, the average of these curves, and the two 'average ± one standard deviation' curves. These average curves are used for analyses in the later sections. Figure 9-c shows the two average bond-slip curves of the free end and loaded end of RAC specimens taken from Figures 9-a and 9-b, respectively, for comparison. It can be seen that these two curves are very close to each other. This shows a relatively small elongation of GFRP bars, providing information for developing models to predict bond-slip behaviour.

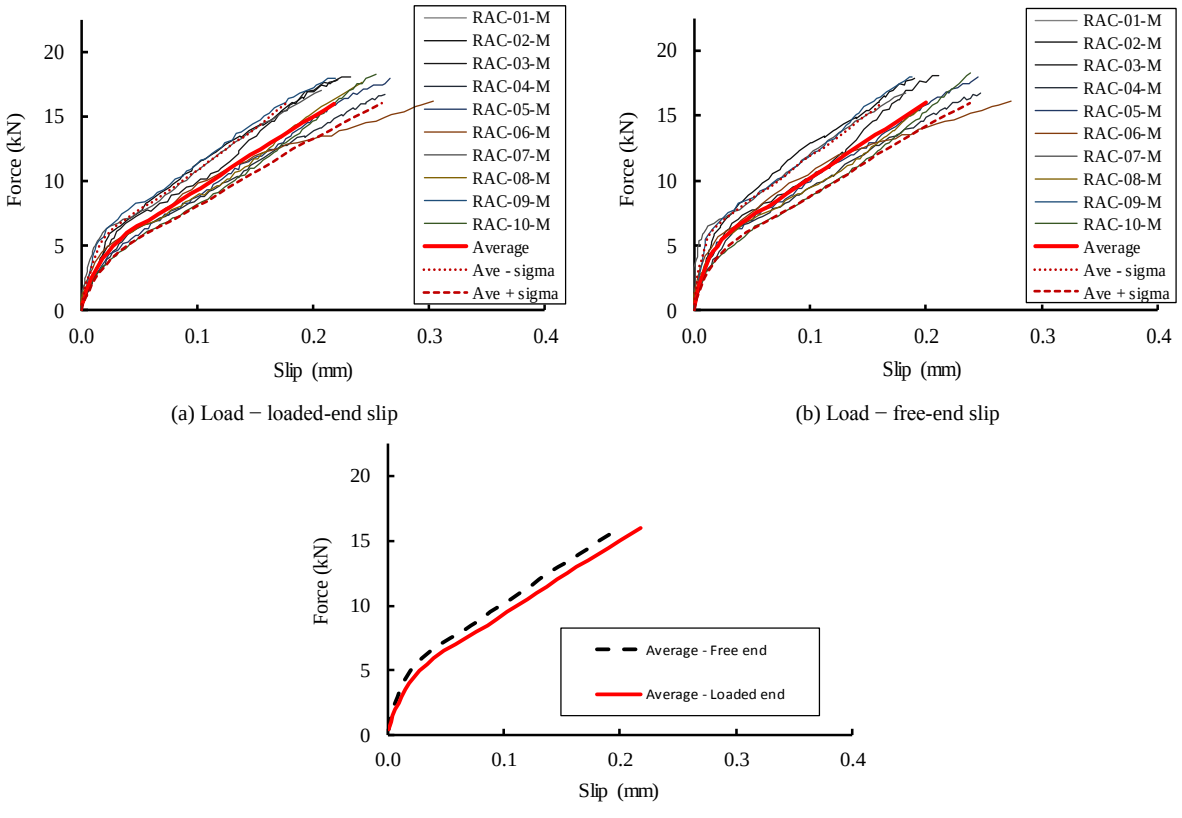

(a) Load − loaded-end slip (b) Load − free-end slip

(c) Average curves

Figure 9. Load – slip curves of RAC group specimens under monotonic loading

Figures 10-a and 10-b show the load-slip curves of the loaded and free ends of specimens NAC-01-M and NAC-02-M under monotonic loading, respectively. The curves can be divided into two branches: branches 1 and 2 when the load is below and above 5 kN, respectively. The stiffness of branch 2 is much smaller than that of branch 1. The procedure to compute the average curves was used, and the obtained average load-slip curves of the loaded and free ends are shown in Figures 10-a and 10-b, respectively. These two average curves are plotted in Figure 10-c for comparison. As can be seen in this figure, these two curves are quite close to each other, showing a small elongation of GFRP bars.

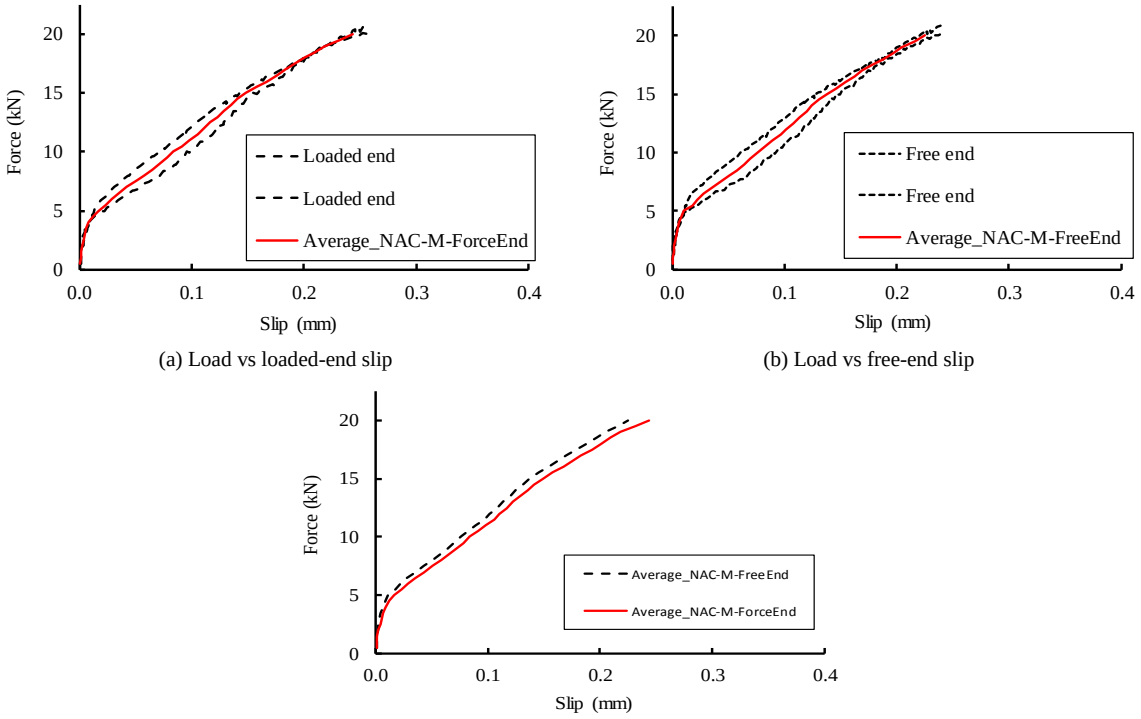

(a) Load vs loaded-end slip

(b) Load vs free-end slip

(c) Average curves

Figure 10. Load-slip curves of NAC group specimens under monotonic loading

Figure 11-a shows the ultimate slips of RAC and NAC specimens under monotonic loading. It can be seen in this Figure that the ultimate slips of RAC specimens vary significantly. The lowest slip is 0.186 mm while the highest slip is 0.304 mm. The average slips of free and loaded ends are 0.227 mm and 0.250 mm (0.238 mm on average), respectively while these two slips have a similar standard deviation of 0.034 mm. The corresponding coefficients of variation (COV) are 0.138 and 0.147 (0.142 on average), respectively, which are relatively high. The average slips of loaded and free ends of NAC specimens are 0.259 mm and 0.239 mm, respectively. Compared with the average slips of NAC specimens, those of RAC specimens are negligibly (3.5%–4.9%) higher. In contrast, the ultimate loads of RAC specimens are quite close to one another as shown in Figure 11-b. The ultimate loads vary from 16.17 kN to 18.27 kN. The average and standard deviation of the ultimate load are 17.56 kN and 0.677 kN, respectively. Correspondingly, COV is 0.039, which is relatively small and is much smaller than COVs of ultimate slips. The ultimate loads of two NAC specimens are 20.18 kN and 20.86 kN; their average value is 20.52 kN. Compared with this average value, the average ultimate load of RAC specimens is 14.4% lower. This lower percentage can be explained by that the strength of RAC are (26.3−22.4)/26.3×100%=14.8% of the strength of NAC.

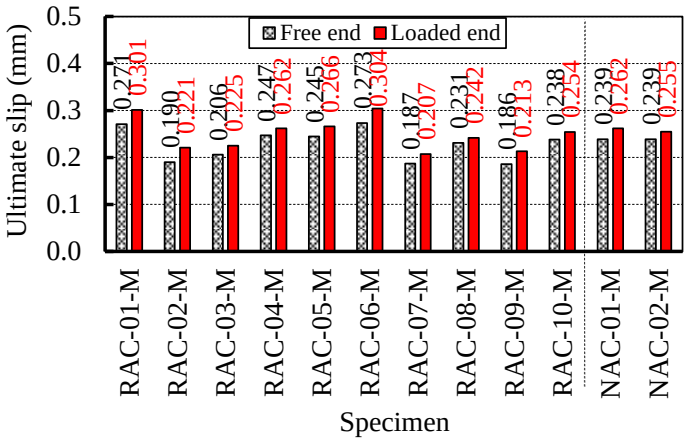

(a) Ultimate slips

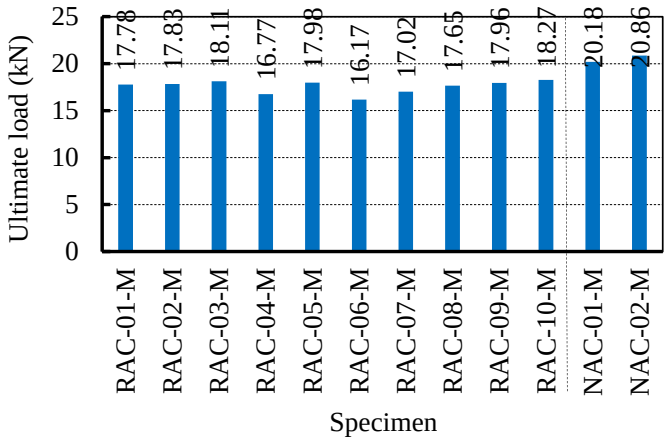

(b) Ultimate loads

Figure 11. Ultimate slips and loads under monotonic loading

Figure 12 compares the average curves of RAC and NAC specimens under monotonic loading. The curves of NAC specimens are higher than those of RAC specimens. It shows that the curves can be divided into two branches: branch 1 can be a parabola up to around 5 kN and branch 2 is from 5 kN to the ultimate. It is worth noting that this characteristic was also found for the case of cyclic loading presented in the later section.

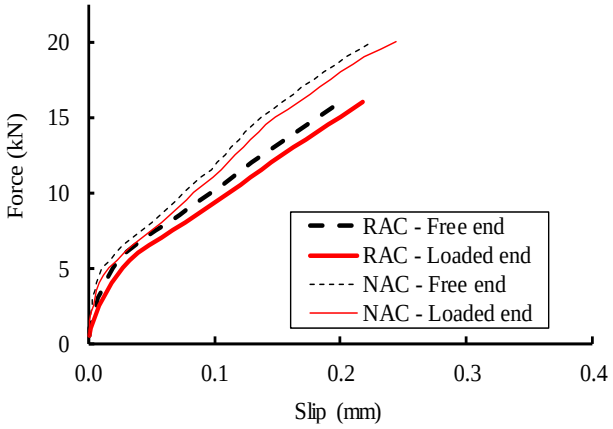

Figure 12. Comparisons of average load-slip curves

4.2. Envelop Load–Slip Curves under Cyclic Loading

Envelop curves of the cyclic behaviours presented in Figure 8 were determined and used in this section. Figure 13a shows ten envelop load-loaded-end slip curves of specimens. These curves were used to compute the average and 'average ± one standard deviation' curves, which were plotted as the red curves in this figure. Figure 13b presents similar curves, but these are of free ends. The two average curves in Figures 13-a, and 13-b are plotted in Figure 13c for comparison. As can be seen in Figure 13-c, the two curves are very close to each other. These average curves are used for analysis in the later sections.

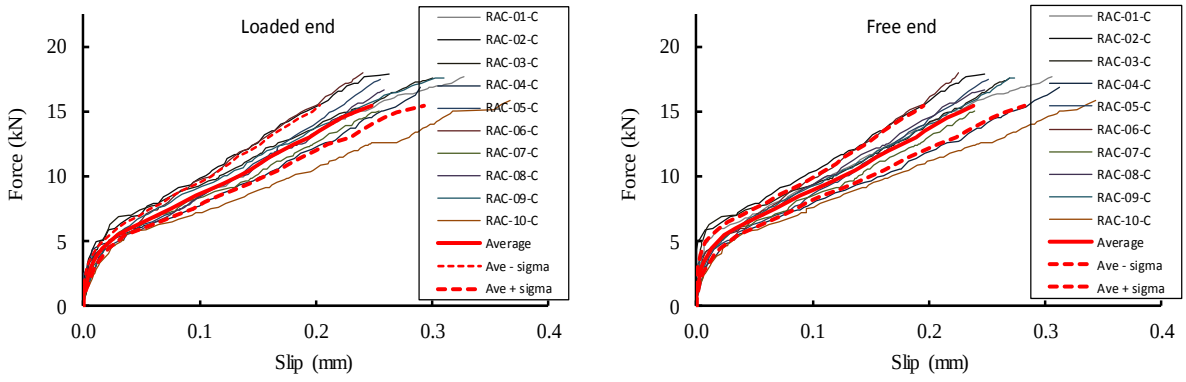

(a) Load vs. loaded-end slip

(b) Load vs. free-end slip

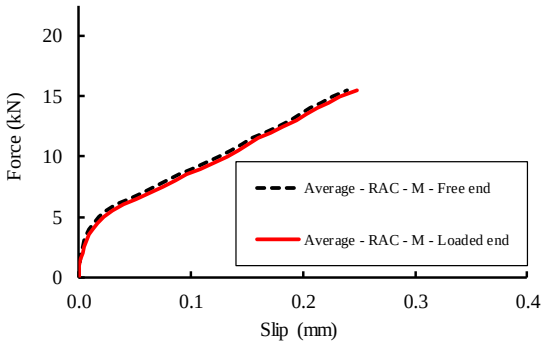

(c) Average envelope load-slip curves

Figure 13. Envelop load-slip curves of RAC group specimens under cyclic loading

Figure 14-a shows the envelop load–slip curves of loaded ends of NAC specimens (NAC-01-C and NAC-02-C) and their average curve, while Figure 14-b shows those of free ends of these specimens. The average load–slip curves exhibit two stages which are divided by the load of approximately 5 kN. The stiffness of the first branch is much higher than that of the second branch. Figure 14-c shows a comparison of these two averages envelop curves. It can be seen that these two average curves are quite close to each other, which shows the axial deformation of the FRP bar is small while the slip can mainly depend on the concrete and the resin.

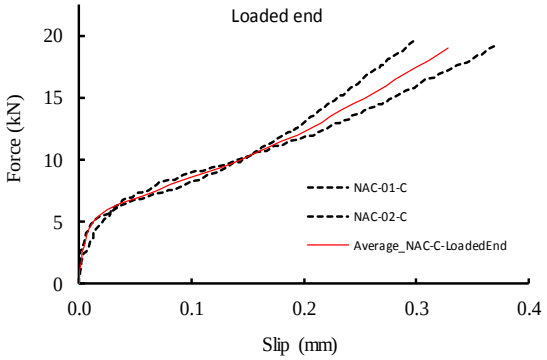

(a) Envelop load-loaded-end slip curves

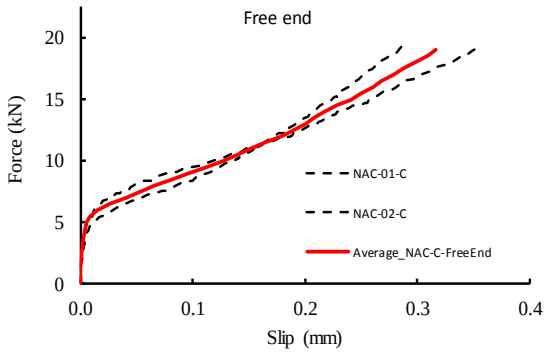

(b) Envelop load-free-end slip curves

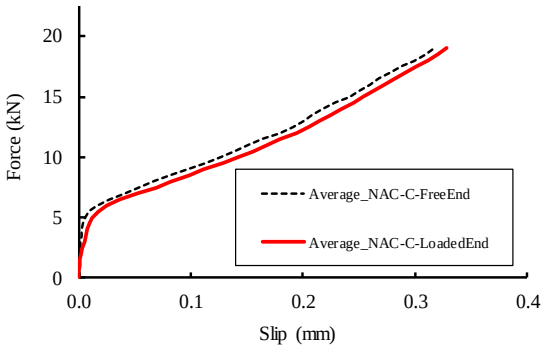

(c) Average envelop curves

Figure 14. Envelop load-slip curves of NAC group specimens under cyclic loading

Figure 15-a shows the ultimate slips of loaded and free ends of specimens under cyclic loading. Overall, the ultimate slips vary significantly from 0.226 mm to 0.367 mm. The average slips of free and loaded ends of RAC specimens under cyclic loading are 0.276 mm and 0.291 mm (0.284 mm on average), respectively. The standard deviations of these slips are 0.036 mm and 0.038 mm; therefore, the corresponding COVs are 0.130 and 0.131 respectively. Figure 15-a shows the ultimate slips of NAC specimens, which vary from 0.292 mm to 0.372 mm. The average ultimate slips of free and loaded ends of these specimens are 0.324 mm and 0.335 mm, which are 14.8% and 13.0% lower than those of NAC specimens, respectively. In contrast, the ultimate loads of specimens seem to be close to one another as shown in Figure 15-b. The ultimate loads of RAC specimens vary from 15.83 kN to 17.99 kN. The average and standard deviation of these loads are 19.43 kN and 0.66 kN, respectively; therefore, COV is 0.038, which is relatively small and much lower than that of the ultimate slips as mentioned above. Moving on NAC specimens, the ultimate loads of NAC-01-C and NAC-02-C are 19.56 kN and 19.29 kN (19.43 kN on average), respectively. Therefore, the average ultimate load of RAC specimens is 10.8% lower than that of NAC specimens. The above lower percentages can be attributed to that the strength of NAC is 14.8% lower than that of RAC.

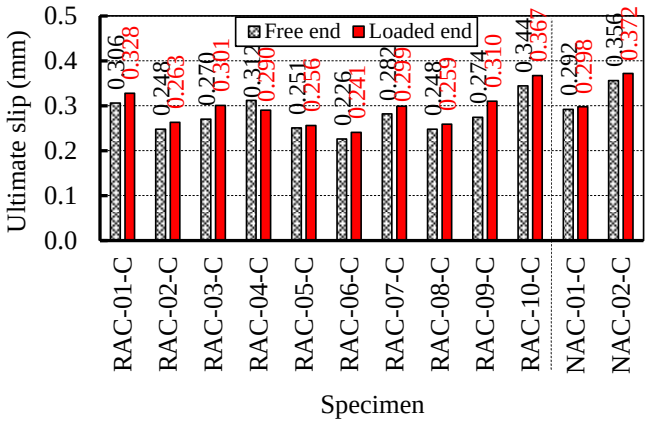

(a) Ultimate slips

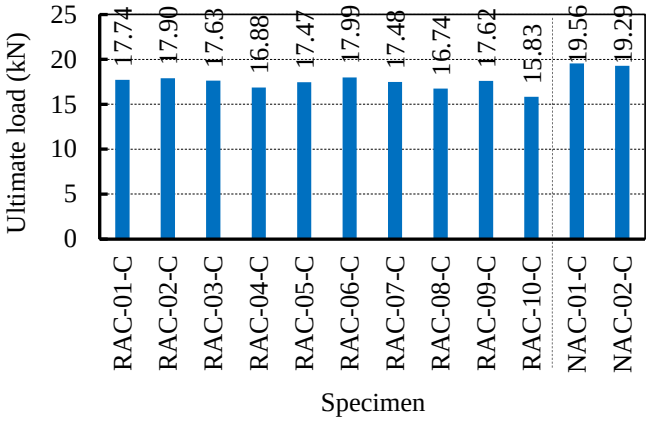

(b) Ultimate load

Figure 15. Ultimate slips and loads under cyclic loading

4.3. Absorbed Energy under Cyclic Loading

Figure 16 shows the variations of absorbed energy with respect to the number of cycles. The calculation of absorbed energy was conducted in MATLAB using area method, which is described as follows. The infinitesimal area A_j under the curve and between loading steps j and $j + 1$ was computed. For the loading curve, this area was added to the energy function $E_j = E_{j-1} + A_j$. It is noted that initial energy E_0 is zero. For the unloading curve, this infinitesimal area A_j was subtracted from the energy function. This calculation procedure was carried out until the ultimate. Based on the energy function obtained, the energy corresponding to each cycle was determined and plotted in Figure 16. It is clearly shown in Figure 16 that the average energy curve of NAC specimens is much higher than that of RAC specimens. During the first cycle, the absorbed energy is almost zero, whereas it started to increase in the second cycle. Then, the absorbed energy significantly increased from the cycle 3 to the ultimate. It is worth noting that the peak load of cycle 2 is 5 kN, which is corresponding to the point that divided the bond–slip behaviour into two branches. The phenomenon is attributed to the larger unrecoverable deformation of specimens in the second phase (after 5 kN).

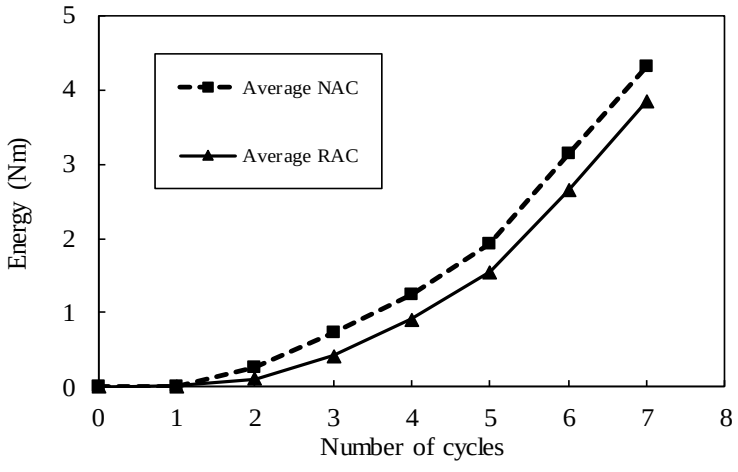

Figure 16. Absorbed energy

4.4. Analyses of Cyclic Loading Effects on RAC Ultimate Slip, Ultimate Load, and Stiffness

The effects of cyclic loading on ultimate slip, ultimate load, and stiffness are shown in Table 3. The ultimate slip significantly increases by 19.3%; however, the ultimate load is marginally reduced by 1.3%. The significant increase in ultimate slip but marginal decrease in ultimate load leads to a significant reduction in stiffness. The stiffness of the second branch of RAC specimens under monotonic and cyclic loadings is 57.81 kN/mm and 46.58 kN/mm, respectively. Therefore, the effect of cyclic loading decreased the stiffness by 19.4%.

Table 3. Effects of cyclic loading

Group	Parameter	Monotonic	Cyclic	%
RAC	Ultimate slip (mm)	0.238	0.284	**19.3**
	Ultimate load (kN)	17.56	17.33	**-1.3**
	Stiffness of second branch (kN/mm)	57.81	46.58	**-19.4**

5. Failure Theory and the Modified Model

5.1. Failure Theory

Figure 17-a shows a simple illustration of a NSM FRP bar in a reinforced concrete block. The FRP bar is bonded to resin, and then the resin is bonded to cover the concrete. It should be noted that concrete in a reinforced concrete block can be divided into two portions: 1) concrete surrounded by steel reinforcement, which is called reinforced concrete (the dashed area in Figure 17-a), and 2) cover concrete, which is called concrete for short. The concrete portion shown in Figure 17-a is considered to be fixed to reinforced concrete. Because the strength of resin is much larger than that of concrete, the failure surface is thus in concrete between the resin and reinforced concrete. This agrees with the failure observed in the tests as described in Section 3.1.

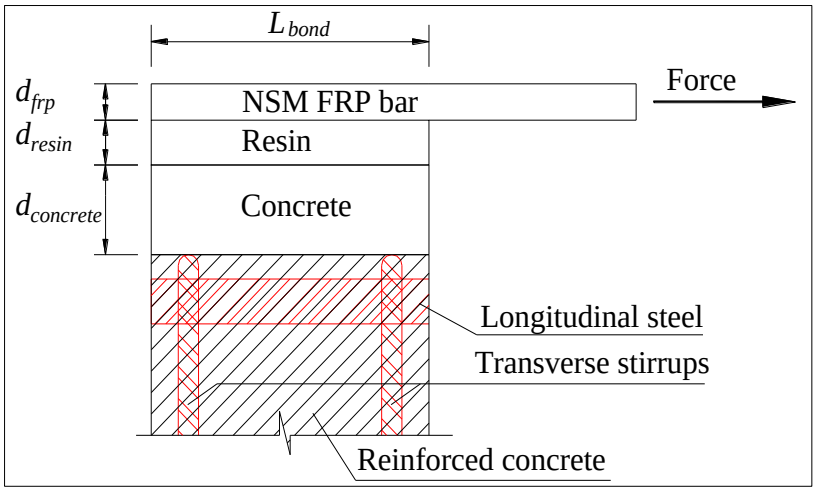

(a) Illustration of NSM FRP

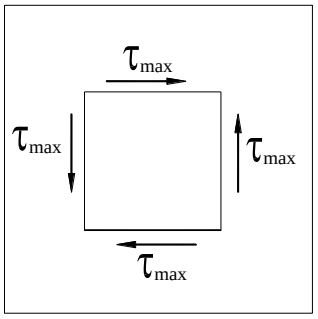

(b) A concrete element under pure shear stress

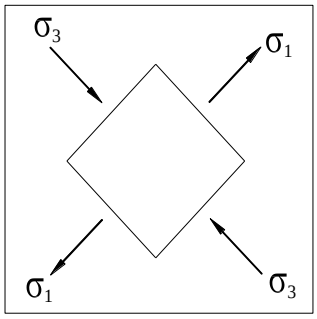

(c) Stress transformation and failure surface

Figure 17. Failure theory

Concrete shown in Figure 17-a can be approximately modelled by elements under pure shear stress state as shown in Figure 17-b and its principal element is shown in Figure 17-c. The principal stresses σ_1 and σ_3 are determined as follows: $\sigma_1 = \tau_{max}$ (tension) and $\sigma_3 = -\tau_{max}$ (compression). When the tension stress σ_1 reaches the tensile strength (f'_t) of

concrete, failure of concrete occurs. Therefore, $\tau_{max} = \sigma_1 = f'_t$ is used as a criterion for the failure of specimens. The tensile strength of concrete should be less than 20% of the compressive strength [58] as shown in Equation 3, in which $k \leq 0.2$. The rough value of tensile strength of concrete can commonly be taken as $0.1f'_c$. The tensile strength of concrete adopted in FIB MC 2010 [59] is determined by Equation 4. ACI 318-19 [60] recommended the Equation 5 for the tensile strength of concrete. These values of tensile strength of concrete are used in Sections 5.2 and 5.3.

$$f_t = kf'_c \quad (3)$$

$$f_t = 0.3f'^{2/3}_c \quad (4)$$

$$f_t = 0.62\sqrt{f'_c} \quad (5)$$

5.2. Modified Model

In this section, the original bond–slip model of steel bars in concrete [59] is presented; then, its parameters are modified to suit the behaviour of NSM GFRP in RAC. Comité Euro-International du Béton and Fédération Internationale de la Précontrainte (CEB-FIP) [59] used Equation 6 as the model of bond–slip behaviour of steel in concrete, in which s (mm) is the slip; α = 0.4 and 0.5 for deformed and plain steel bars, respectively; τ_{max} is the shear bond strength; s_{max} is the ultimate slip; and α is a parameter defining the shape of the curve.

$$\tau = \tau_{max}\left(\frac{s}{s_{max}}\right)^{\alpha} \quad (6)$$

The above model is modified by redefining its parameters to suit the case of NSM GFRP bars in reinforced RAC. The maximum slip is taken to be s_{max} = 0.25 mm, which is close to the average ultimate slips of the tested specimens; $\tau_{max} = f_t$, which is equal to the ultimate shear stress of concrete; α is selected to be 0.5.

5.3. Validation of the Modified Model

Prior to validation, the experimental load–slip curves are converted to stress–slip curves by dividing the load by the shear surface area of concrete $A_c = 3 \times d_{groove} \times L_{bond}$, in which d_{groove} is the dimension of grooves, L_{bond} is the bond length and 3 is the three surfaces of concrete contacting with resin. Figure 18 shows the average slip–stress curves of RAC specimens. These curves clearly include two parts: part 1 from zero to about 1 MPa and part 2 from 1 MPa to ultimate. This shape can be explained by the following mechanism. At a small shear stress, the slip is very small, and materials work in their elastic range with their initial shear modulus. When the shear stress increases, the shear modulus decreases to some extents. Additionally, this stress causes micro cracks which reduce the stiffness of specimens. The point where the curves change the stiffness can be considered as the 'micro cracking' point, at which micro cracking occurred in the concrete region close to the resin and FRP bars. Moreover, because the load–slip curves of free and loaded ends are very close to each other, the average curve of these two curves was computed and used for verification.

Figure 18-a shows the comparisons between the bond-slip curves of the modified model and the curve obtained from experiments in the case of monotonic loading. Figure 18-b shows a similar comparison, but for the case of cyclic loading. Using the tensile strength recommended by ACI 318-19 [60], the modified model exhibited an overall match with the experimental results; however, there is a difference at the end of the curve when the load approaches the ultimate in the case of monotonic loading. In the case of cyclic loading, the difference is in the middle of the curve. These differences are because the curve is expressed by a smooth equation, which is normally difficult to match in the whole domain. Using the tensile strength recommended by FIB MC 2010 [59] or the rough value of 10% of the compressive concrete strength results in conservative bond-slip behaviour compared with the experimental curves. These two curves are very close to each other and tend to be safe for design.

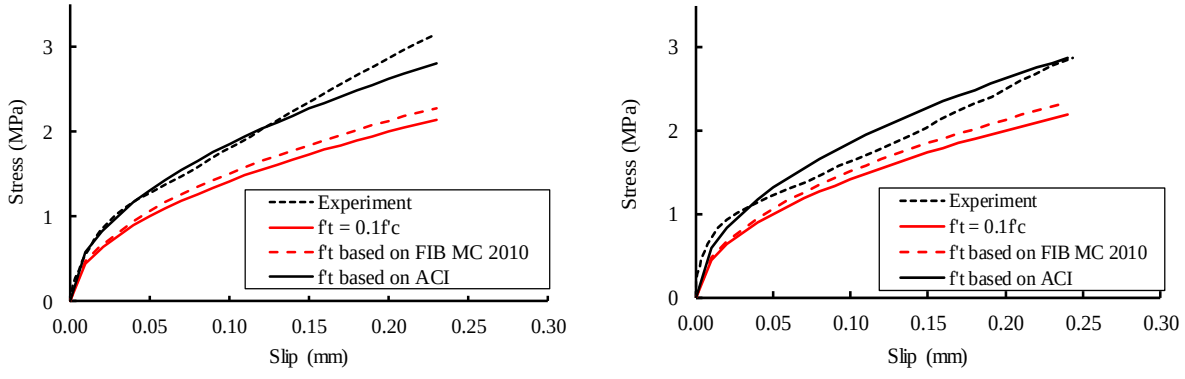

(a) Under monotonic loading (b) Under cyclic loading

Figure 18. Comparison of bond–slip behaviour of RAC: model vs. experiment

6. Conclusions

The following conclusions are presented based on the obtained results:

- The majority of specimens failed in the form of brittle shear failure of concrete in the proximity of a resin-concrete surface. The failure process occurred rapidly, resulting in the disintegration of the concrete into pieces. Brittle failure resulted in a sudden drop in load to zero, a characteristic that needs to be avoided in retrofitting designs.
- The bond-slip behaviour could be characterized by two stages: nonlinear and linear. However, the nonlinear portion was within 25% of the ultimate load and within a relatively small slip, whereas the linear portion was a non-descending branch, which dominated the bond-slip behaviour. Due to the domination of the linear portion, the whole behaviour could be approximated by a straight line for rough modelling purposes; however, investigation on this idea needs be further investigated.
- The average ultimate slip of RAC specimens was up to 14.8% lower than that of NAC specimens. The average slips of RAC specimens under monotonic and cyclic loadings were 0.238 mm and 0.284 mm, and COVs were relatively large at 0.142 and 0.130, respectively. In contrast, the ultimate loads of RAC specimens had a low COV of 0.038. The ultimate loads of RAC specimens under monotonic and cyclic loadings were 14.4% and 10.8% lower than those of NAC specimens, respectively. These lower percentages can be explained by that the strength of RAC are (26.3−22.4)/26.3×100%=14.8% of the strength of NAC.
- The effect of cyclic loading significantly increased the ultimate slips by 19.3%, whereas it marginally reduced the ultimate load by 1.3%; consequently, the stiffness was reduced by 19.4%. Therefore, stiffness degradation should be considered in NSM GFRP retrofitting of reinforced RAC under cyclic loading.
- The modified smooth model was proposed to estimate the bond-slip behaviour of NSM GFRP bars in reinforced RAC. The modified model is simple because its parameters are easy to determine, whereas it exhibited good agreement with the experimental results. The simplicity and accuracy of the model can be useful for engineers in modeling reinforced RAC structures retrofitted with the NSM FRP technique.

7. Declarations

7.1. Author Contributions

Conceptualization, A.T.L. and V.V.C.; methodology, A.T.L., and T.N.N.; formal analysis, A.T.L., T.N.N., and V.V.C.; investigation, A.T.L., and V.V.C.; resources, A.T.L., and T.N.N.; data curation, V.V.C.; writing—original draft preparation, V.V.C.; writing—review and editing, A.T.L., T.N.N., and V.V.C.; visualization, T.N.N., and V.V.C.; supervision, T.N.N. All authors have read and agreed to the published version of the manuscript.

7.2. Data Availability Statement

The data presented in this study are available in the article.

7.3. Funding and Acknowledgement

The authors acknowledge Ho Chi Minh City University of Technology (HCMUT), VNU-HCM for supporting this study.

7.4. Conflicts of Interest

The authors declare no conflict of interest.

8. References

[1] Mansour, M., & El-Maaddawy, T. (2021). Testing and modeling of deep beams strengthened with NSM-CFRP reinforcement around cutouts. Case Studies in Construction Materials, 15. doi:10.1016/j.cscm.2021.e00670.

[2] Imjai, T., Setkit, M., Garcia, R., & Figueiredo, F. P. (2020). Strengthening of damaged low strength concrete beams using PTMS or NSM techniques. Case Studies in Construction Materials, 13. doi:10.1016/j.cscm.2020.e00403.

[3] Obaidat, Y. T., Barham, W. S., Obaidat, A. T., & Attar, K. M. (2021). Behavior of NSM CFRP reinforced concrete columns: Experimental and analytical work. Case Studies in Construction Materials, 15. doi:10.1016/j.cscm.2021.e00589.

[4] Seifi, A., Hosseini, A., Marefat, M. S., & Zareian, M. S. (2017). Improving seismic performance of old-type RC frames using NSM technique and FRP jackets. Engineering Structures, 147, 705–723. doi:10.1016/j.engstruct.2017.06.034.

[5] Panahi, M., Zareei, S. A., & Izadi, A. (2021). Flexural strengthening of reinforced concrete beams through externally bonded FRP sheets and near surface mounted FRP bars. Case Studies in Construction Materials, 15. doi:10.1016/j.cscm.2021.e00601.

[6] Bilotta, A., Ceroni, F., Di Ludovico, M., Nigro, E., Pecce, M., & Manfredi, G. (2011). Bond Efficiency of EBR and NSM FRP Systems for Strengthening Concrete Members. Journal of Composites for Construction, 15(5), 757–772. doi:10.1061/(asce)cc.1943-5614.0000204.

[7] Bilotta, A., Ceroni, F., Nigro, E., & Pecce, M. (2014). Strain assessment for the design of NSM FRP systems for the strengthening of RC members. Construction and Building Materials, 69, 143–158. doi:10.1016/j.conbuildmat.2014.07.024.

[8] Dias, S. J. E., Barros, J. A. O., & Janwaen, W. (2018). Behavior of RC beams flexurally strengthened with NSM CFRP laminates. Composite Structures, 201, 363–376. doi:10.1016/j.compstruct.2018.05.126.

[9] Lu, X. Z., Teng, J. G., Ye, L. P., & Jiang, J. J. (2005). Bond-slip models for FRP sheets/plates bonded to concrete. Engineering Structures, 27(6), 920–937. doi:10.1016/j.engstruct.2005.01.014.

[10] Teng, J. G., Zhang, S. S., Dai, J. G., & Chen, J. F. (2013). Three-dimensional meso-scale finite element modeling of bonded joints between a near-surface mounted FRP strip and concrete. Computers and Structures, 117, 105–117. doi:10.1016/j.compstruc.2012.12.002.

[11] Hassan, T., & Rizkalla, S. (2003). Investigation of Bond in Concrete Structures Strengthened with Near Surface Mounted Carbon Fiber Reinforced Polymer Strips. Journal of Composites for Construction, 7(3), 248–257. doi:10.1061/(asce)1090-0268(2003)7:3(248).

[12] de Sena Cruz, J. M., & Oliveira de Barros, J. A. (2004). Bond Between Near-Surface Mounted Carbon-Fiber-Reinforced Polymer Laminate Strips and Concrete. Journal of Composites for Construction, 8(6), 519–527. doi:10.1061/(asce)1090-0268(2004)8:6(519).

[13] Rashid, R., Oehlers, D. J., & Seracino, R. (2008). IC Debonding of FRP NSM and EB Retrofitted Concrete: Plate and Cover Interaction Tests. Journal of Composites for Construction, 12(2), 160–167. doi:10.1061/(asce)1090-0268(2008)12:2(160).

[14] Oehlers, D. J., Haskett, M., Wu, C., & Seracino, R. (2008). Embedding NSM FRP Plates for Improved IC Debonding Resistance. Journal of Composites for Construction, 12(6), 635–642. doi:10.1061/(asce)1090-0268(2008)12:6(635).

[15] Vasquez, D., & Seracino, R. (2010). Assessment of the predictive performance of existing analytical models for debonding of near-surface mounted FRP strips. Advances in Structural Engineering, 13(2), 299–308. doi:10.1260/1369-4332.13.2.299.

[16] Zhang, S. S., Teng, J. G., & Yu, T. (2013). Bond-slip model for CFRP strips near-surface mounted to concrete. Engineering Structures, 56, 945–953. doi:10.1016/j.engstruct.2013.05.032.

[17] Zhang, S. S., Teng, J. G., & Yu, T. (2014). Bond Strength Model for CFRP Strips Near-Surface Mounted to Concrete. Journal of Composites for Construction, 18(3). doi:10.1061/(asce)cc.1943-5614.0000402.

[18] Dai, J., Ueda, T., & Sato, Y. (2005). Development of the Nonlinear Bond Stress–Slip Model of Fiber Reinforced Plastics Sheet–Concrete Interfaces with a Simple Method. Journal of Composites for Construction, 9(1), 52–62. doi:10.1061/(asce)1090-0268(2005)9:1(52).

[19] De Lorenzis, L., & Nanni, A. (2002). Bond between near-surface mounted fiber-reinforced polymer rods and concrete in structural strengthening. ACI Structural Journal, 99(2), 123–132. doi:10.14359/11534.

[20] De Lorenzis, L., Rizzo, A., & La Tegola, A. (2002). A modified pull-out test for bond of near-surface mounted FRP rods in concrete. Composites Part B: Engineering, 33(8), 589–603. doi:10.1016/S1359-8368(02)00052-5.

[21] Galati, D., & De Lorenzis, L. (2009). Effect of construction details on the bond performance of NSM FRP bars in concrete. Advances in Structural Engineering, 12(5), 683–700. doi:10.1260/136943309789867836.

[22] Soliman, S. M., El-Salakawy, E., & Benmokrane, B. (2011). Bond Performance of Near-Surface-Mounted FRP Bars. Journal of Composites for Construction, 15(1), 103–111. doi:10.1061/(asce)cc.1943-5614.0000150.

[23] Sharaky, I. A., Torres, L., Baena, M., & Vilanova, I. (2013). Effect of different material and construction details on the bond behaviour of NSM FRP bars in concrete. Construction and Building Materials, 38, 890–902. doi:10.1016/j.conbuildmat.2012.09.015.

[24] Sharaky, I. A., Torres, L., Baena, M., & Miàs, C. (2013). An experimental study of different factors affecting the bond of NSM FRP bars in concrete. Composite Structures, 99, 350–365. doi:10.1016/j.compstruct.2012.12.014.

[25] Kalupahana, W. K. K. G., Ibell, T. J., & Darby, A. P. (2013). Bond characteristics of near surface mounted CFRP bars. Construction and Building Materials, 43, 58–68. doi:10.1016/j.conbuildmat.2013.01.021.

[26] Lee, D., Cheng, L., & Yan-Gee Hui, J. (2013). Bond Characteristics of Various NSM FRP Reinforcements in Concrete. Journal of Composites for Construction, 17(1), 117–129. doi:10.1061/(asce)cc.1943-5614.0000318.

[27] Caro, M., Jemaa, Y., Dirar, S., & Quinn, A. (2017). Bond performance of deep embedment FRP bars epoxy-bonded into concrete. Engineering Structures, 147, 448–457. doi:10.1016/j.engstruct.2017.05.069.

[28] Gómez, J., Torres, L., & Barris, C. (2020). Characterization and simulation of the bond response of NSM FRP reinforcement in Concrete. Materials, 13(7), 1770. doi:10.3390/MA13071770.

[29] Gómez, J., Barris, C., Jahani, Y., Baena, M., & Torres, L. (2021). Experimental study and numerical prediction of the bond response of NSM CFRP laminates in RC elements under sustained loading. Construction and Building Materials, 288, 123082. doi:10.1016/j.conbuildmat.2021.123082.

[30] Zhang, R., & Xue, X. (2021). A predictive model for the bond strength of near-surface-mounted FRP bonded to concrete. Composite Structures, 262, 113618. doi:10.1016/j.compstruct.2021.113618.

[31] Slaitas, J., & Valivonis, J. (2021). Bond strength evaluation methods of RC members strengthened with FRP composites. Engineering Structures, 249, 113357. doi:10.1016/j.engstruct.2021.113357.

[32] Wang, X., & Cheng, L. (2021). Bond characteristics and modeling of near-surface mounted CFRP in concrete. Composite Structures, 255, 113011. doi:10.1016/j.compstruct.2020.113011.

[33] Aghamohammadi, R., Nasrollahzadeh, K., Mofidi, A., & Gosling, P. (2021). Reliability-based assessment of bond strength models for near-surface mounted FRP bars and strips to concrete. Composite Structures, 272, 114132. doi:10.1016/j.compstruct.2021.114132.

[34] Li, L., Mai, G., He, S., Xiong, Z., Wei, W., Luo, H., & Liu, F. (2021). Experimental study on bond behaviour between recycled aggregate concrete and basalt fibre-reinforced polymer bars under different strain rates. Construction and Building Materials, 290, 123218. doi:10.1016/j.conbuildmat.2021.123218.

[35] Yazdani, A., Sanginabadi, K., Shahidzadeh, M. S., Salimi, M. R., & Shamohammadi, A. (2021). Consideration of data correlation to estimate FRP-to-concrete bond capacity models. Construction and Building Materials, 308, 125106. doi:10.1016/j.conbuildmat.2021.125106.

[36] Mosallam, A. S., Ghabban, N., Mirnateghi, E., & Agwa, A. A. K. (2022). Nonlinear numerical simulation and experimental verification of bondline strength of CFRP strips embedded in concrete for NSM strengthening applications. Structural Concrete, 23(3), 1794–1815. doi:10.1002/suco.202100537.

[37] Aljidda, O., El Refai, A., & Alnahhal, W. (2023). Comparative study on the bond performance of near-surface mounted fiber-reinforced polymer bars. Construction and Building Materials, 364, 129923. doi:10.1016/j.conbuildmat.2022.129923.

[38] Sanginabadi, K., Yazdani, A., Mostofinejad, D., & Czaderski, C. (2022). RC members externally strengthened with FRP composites by grooving methods including EBROG and EBRIG: A state-of-the-art review. Construction and Building Materials, 324, 126662. doi:10.1016/j.conbuildmat.2022.126662.

[39] Abbas, A., Fathifazl, G., Isgor, O. B., Razaqpur, A. G., Fournier, B., & Foo, S. (2009). Durability of recycled aggregate concrete designed with equivalent mortar volume method. Cement and Concrete Composites, 31(8), 555–563. doi:10.1016/j.cemconcomp.2009.02.012.

[40] Casuccio, M., Torrijos, M. C., Giaccio, G., & Zerbino, R. (2008). Failure mechanism of recycled aggregate concrete. Construction and Building Materials, 22(7), 1500–1506. doi:10.1016/j.conbuildmat.2007.03.032.

[41] Eguchi, K., Teranishi, K., Nakagome, A., Kishimoto, H., Shinozaki, K., & Narikawa, M. (2007). Application of recycled coarse aggregate by mixture to concrete construction. Construction and Building Materials, 21(7), 1542–1551. doi:10.1016/j.conbuildmat.2005.12.023.

[42] Ismail, S., Kwan, W. H., & Ramli, M. (2017). Mechanical strength and durability properties of concrete containing treated recycled concrete aggregates under different curing conditions. Construction and Building Materials, 155(Supplement C), 296–306. doi:10.1016/j.conbuildmat.2017.08.076.

[43] Thomas, C., Setién, J., Polanco, J. A., Alaejos, P., & Sánchez De Juan, M. (2013). Durability of recycled aggregate concrete. Construction and Building Materials, 40, 1054–1065. doi:10.1016/j.conbuildmat.2012.11.106.

[44] Lei, B., Li, W., Tang, Z., Tam, V. W. Y., & Sun, Z. (2018). Durability of recycled aggregate concrete under coupling mechanical loading and freeze-thaw cycle in salt-solution. Construction and Building Materials, 163, 840–849. doi:10.1016/j.conbuildmat.2017.12.194.

[45] Tam, V. W. Y., Kotrayothar, D., & Xiao, J. (2015). Long-term deformation behaviour of recycled aggregate concrete. Construction and Building Materials, 100, 262–272. doi:10.1016/j.conbuildmat.2015.10.013.

[46] Jin, R., Li, B., Elamin, A., Wang, S., Tsioulou, O., & Wanatowski, D. (2018). Experimental Investigation of Properties of Concrete Containing Recycled Construction Wastes. International Journal of Civil Engineering, 16(11), 1621–1633. doi:10.1007/s40999-018-0301-4.

[47] Kapoor, K., Singh, S. P., & Singh, B. (2018). Water Permeation Properties of Self Compacting Concrete Made with Coarse and Fine Recycled Concrete Aggregates. International Journal of Civil Engineering, 16(1), 47–56. doi:10.1007/s40999-016-0062-x.

[48] Etxeberria, M., & Gonzalez-Corominas, A. (2018). Properties of Plain Concrete Produced Employing Recycled Aggregates and Sea Water. International Journal of Civil Engineering, 16(9), 993–1003. doi:10.1007/s40999-017-0229-0.

[49] Liu, F., Yu, Y. Y., Li, L. J., & Zeng, L. (2018). Experimental study on reuse of recycled concrete aggregates for load-bearing components of building structures. Journal of Material Cycles and Waste Management, 20(2), 995–1005. doi:10.1007/s10163-017-0661-x.

[50] Xu, J. J., Chen, Z. P., Ozbakkaloglu, T., Zhao, X. Y., & Demartino, C. (2018). A critical assessment of the compressive behavior of reinforced recycled aggregate concrete columns. Engineering Structures, 161, 161–175. doi:10.1016/j.engstruct.2018.02.003.

[51] Fan, Y. J., Yu, B. S., & Wang, S. L. (2018). Analysis and Evaluation of the Stochastic Damage for Recycled Aggregate Concrete Frames under Seismic Action. International Journal of Civil Engineering, 16(7), 783–791. doi:10.1007/s40999-017-0203-x.

[52] TCVN 7570. (2006). Aggregates for concrete and mortar (Technical Requirements). Vietnam Construction Standards, Hanoi, Vietnam. (In Vietnamese).

[53] Ceroni, F., Pecce, M., Bilotta, A., & Nigro, E. (2012). Bond behavior of FRP NSM systems in concrete elements. Composites Part B: Engineering, 43(2), 99–109. doi:10.1016/j.compositesb.2011.10.017.

[54] Ceroni, F., Barros, J. A. O., Pecce, M., & Ianniciello, M. (2013). Assessment of nonlinear bond laws for near-surface-mounted systems in concrete elements. Composites Part B: Engineering, 45(1), 666–681. doi:10.1016/j.compositesb.2012.07.006.

[55] Singh, S. B., Reddy, A. L., & Khatri, C. P. (2014). Experimental and Parametric Investigation of Response of NSM CFRP-Strengthened RC Beams. Journal of Composites for Construction, 18(1), 04013021. doi:10.1061/(asce)cc.1943-5614.0000411.

[56] ACI 440.2R-17. (2017). Guide for the Design and Construction of Externally Bonded FRP Systems for Strengthening Concrete Structures. American Concrete Institute, Farmington Hills, United States.

[57] Ko, H., & Sato, Y. (2007). Bond Stress–Slip Relationship between FRP Sheet and Concrete under Cyclic Load. Journal of Composites for Construction, 11(4), 419–426. doi:10.1061/(asce)1090-0268(2007)11:4(419).

[58] Park, R., & Paulay, T. (1991). Reinforced concrete structures. John Wiley & Sons, Hoboken, United States.

[59] Beton CE-Id. Fib (CEB-FIP). (2012). Model Code 2010 – Final draft, Vol. 1. Fib Bulletin No. 65, International Federation for Structural Concrete (fib), Lausanne, Switzerland.

[60] ACI 318-19. (2019). Building Code Requirements for Structural Concrete. American Concrete Institute, Farmington Hills, United States.